

Solution conformation of the *Pseudomonas syringae* pv. *syringae* phytotoxic lipodepsipeptide syringopeptin 25-A

Two-dimensional NMR, distance geometry and molecular dynamics

Alessandro BALLIO¹, Francesco BOSSA¹, Domenico DI GIORGIO¹, Alfredo DI NOLA², Cesare MANETTI³, Maurizio PACI⁴, Andrea SCALONI¹ and Anna Laura SEGRE⁴

¹ Dipartimento di Scienze Biochimiche 'A. Rossi Fanelli' and Centro di Biologia Molecolare del CNR, Università di Roma 'La Sapienza', Italia

² Dipartimento di Chimica, Università di Roma 'La Sapienza', Italia

³ Istituto di Chimica Biologica, Università di Cagliari e Laboratorio NMR, Università 'Tor Vergata', Roma, Italia

⁴ Istituto di Strutturistica Chimica 'G. Giacomello', CNR, Montelibretti, Roma, Italia

(Received 11 July/9 October 1995) – EJB 95 1129/3

Syringopeptin 25-A is a phytotoxic amphiphilic lipodepsipeptide containing 25 amino acid residues, produced by some isolates of the plant pathogenic bacterium *Pseudomonas syringae* pv. *syringae*. Previous papers have reported its covalent structure and some of its biological properties. Attention has now been directed to define its conformation in solution, a structural feature regarded as important for understanding its possible role in the bacterial colonization of host plants, and its toxic action on the plant cell.

Here we report the stereochemistry of its amino acid components, the complete interpretation of the two-dimensional NMR spectra and NOE data, and finally the structure obtained by computer simulations applying distance geometry and molecular dynamics procedures.

The conformation of syringopeptin 25-A in aqueous solution includes three different structural regions interrupted by rigid 2,3-dehydro-2-aminobutyric acid residues: a loop from residue 2 to 6, a helicoidal zone from 8 to 15, and the lactone ring from 18 to 25. The three-dimensional structure of the lactone moiety is very similar to that of two previously studied bioactive lipodepsinona peptides. Preliminary circular dichroism evidence of conformational variations in solution of trifluoroethanol, which simulates a membrane-like environment, are also reported.

Keywords: NMR; solution structure; molecular dynamics; lipodepsipeptide; syringopeptins.

Syringopeptins are a small group of compounds recently identified among the phytotoxic metabolites of *Pseudomonas syringae* pv. *syringae* (Ballio et al., 1991). These compounds belong to the class of lipodepsipeptides with a marked amphiphilic character and constituted from a long fatty acid chain, a peptide moiety with mixed chirality and a ring with a lactonic closure. The chemical structure of one of this class of compounds was elucidated first in 1985 (Aydin et al., 1985)

Two strains known to produce the lipodepsinona peptide syringomycin synthesize syringopeptin 25-A and 25-B (Fig. 1), which have an identical peptide moiety composed of 25 amino acid residues, and differ from each other in the acyl substituent at the terminal amino group, corresponding to 3-hydroxydecanoic acid in 25-A and to 3-hydroxydodecanoic acid in 25-B. A third syringomycin-producing strain and a syringotoxin-producing strain synthesize syringopeptins 22-A and 22-B (Fig. 1); both have an identical peptide moiety with 22 amino acid residues, while the acyl moiety on the N-terminus corresponds to 3-hydroxydecanoate in 22-A and to 3-hydroxydodecanoate in 22-B. Shortly before the isolation of syringopeptins, two

lipodepsipeptides containing 18 amino acid residues and a 3-hydroxyoctanoyl group, called tolaasin I and II, were purified from culture filtrates of *Pseudomonas tolaasi* and their structures elucidated (Nutkins et al., 1991). Tolaasins are the determinants of brown blotch disease symptoms caused by *P. tolaasi* in the commercially important mushroom *Agaricus bisporus*. They disrupt cellular and subcellular membranes (Rainey et al., 1991), a property shared by syringopeptins (Di Giorgio et al., 1994), and attributable for both groups of compounds to their amphiphilic character. It has been suggested that tolaasins form voltage-gated cation-selective ion channels in planar lipid bilayers, a property arising from peculiar structural features. Tolaasin I, and probably also tolaasin II, show an amphiphilic left-handed α -helix region in solution (Mortishire-Smith et al., 1991a) which, besides additional molecular characteristics, makes it similar to some well studied membrane-active natural peptides.

After having elucidated the chirality of amino acid residues and completely assigned the two-dimensional NMR spectra of syringopeptin 25-A, an extensive collection of NOE data was obtained. The present paper describes the solution conformation determined by distance geometry (DG) computation and molecular dynamics (MD) simulations obtained with the NOE constraints.

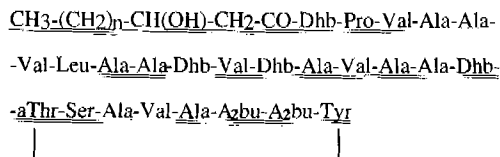
MATERIALS AND METHODS

Syringopeptins. These were prepared and purified as previously reported (Ballio et al., 1991).

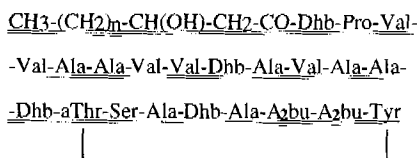
Correspondence to M. Paci, Department of Chemical Sciences and Technology, University of Rome Tor Vergata, Via Ricerca Scientifica, I-00133, Rome, Italy

Fax: +39 6 72594328.

Abbreviations. A₂bu, 2,4-diaminobutyric acid; DG, distance geometry; Dhb, 2,3-dehydro-2-aminobutyric acid; MD, molecular dynamics; NOESY, nuclear Overhauser effect spectroscopy; aThr, allothreonine; TOCSY, total correlated spectroscopy.



SP₂₅A n=6 SP₂₅B n=8



SP₂₂A n=6 SP₂₂B n=8

Fig. 1. Primary structures of syringopeptins 25-A, 25-B, 22-A and 22-B. Common regions have been doubly underlined.

Chirality determination of the amino acid residues of syringopeptins. Partial acid hydrolysis was performed with 60 mM HCl at 110°C for 1–5 h. The resulting peptides were fractionated by reverse-phase (RP) HPLC on an Aquapore RP300 column (7.0×250 mm, 7 μm, Applied Biosystems) eluted with a linear gradient of 0.1% trifluoroacetic acid in acetonitrile/2-propanol (4:1, by vol.) to 0.2% trifluoroacetic acid, flow rate 1.6 ml/min. Selected fractions were purified further on an Aquapore RP300 column (4.6×250 mm, 7 μm, Applied Biosystems) eluted with the same solvents and an appropriate gradient at a flow rate of 0.8 ml/min. Peptide sequences were determined by automated Edman degradation using an Applied Biosystems model 476A protein sequencer. The presence of 2,3-dehydro-2-aminobutyric acid residues was determined according to Scaloni et al. (1994). Chiral analyses of individual amino acids and N-terminal residues were performed as previously described (Marfey, 1984; Scaloni et al., 1991).

CD spectroscopy. CD spectra were obtained using a Jasco J 500A spectropolarimeter, equipped with a DP 520 processor, at a 0.125 mM peptide concentration, pH 7, 25°C, in a 0.1-cm pathlength cell.

NMR spectroscopy. Samples for NMR studies were prepared by dissolving about 1 mg lyophilized sample in 0.5 ml of either D₂O or H₂O/D₂O (9:1, by vol.). NMR spectra of syringopeptin 25-A in diluted HCl, pH 3.6, were run at 25°C on a Bruker AM 400 instrument, operating at 400.13 MHz.

Two-dimensional NMR experiments were performed in the phase-sensitive mode with the time-proportional phase increment phase cycle (Marion and Wüthrich, 1983) typically using 2 K of memory for 512 increments. The number of scans were optimized in order to obtain a satisfactory signal/noise ratio.

Correlation experiments were performed with total correlation experiments (TOCSY), where the spinlock composite pulse sequence has been inserted (Levitt et al., 1982; Braunschweiler and Ernst, 1983) with a typical mixing time of either 16 or 80 ms in order to observe either direct or direct and remote connectivities.

NOE dipolar correlated two-dimensional spectra were obtained using the NOESY pulse sequence (Jeener et al., 1979). The mixing time for the magnetization exchange ranged over 100–300 ms.

Data were processed on a microVax II with the TRITON two-dimensional NMR software produced by Boelens and Vuisiter in 1990 in Utrecht (courtesy of Professor R. Kaptein). Free induction decays were weighted by a sinebell apodization function shifted typically $\pi/3$ in both dimensions.

In all homonuclear two-dimensional experiments, a matrix 1024×1024 in the phase-sensitive mode was thus obtained with a digital resolution of about 5 Hz/point. A baseline correction was made in both dimensions using a polynomial fit routine present in the same program.

Computer simulations. The search for the structure that accounts for the experimental NOEs was performed combining distance geometry (DG) and molecular dynamics (MD).

Distance geometry. This was performed using the DGEOM program of Blaney, Crippen, Dearing and Scott Dixon, licensed in 1990 from QCPE and based on the EMBED algorithm (Crippen, 1983). For the DG calculation the NOE intensity was converted into distance information according to Williamson et al. (1985): the interresidue NOEs were uniformly converted into an upper bound at 0.4 nm distance; the intraresidue NOEs were classified as strong, medium/strong, medium, medium/weak and weak and translated into upper bounds of 0.25, 0.30, 0.35, 0.38 and 0.40 nm, respectively. All the experimental NOEs were used except those sequential between C β Hi and NH(*i*+1), since the absence of stereospecific assignments made them uninformative (Wüthrich et al., 1983).

For coordinate optimization a maximum violation of 0.10 nm for distances and 0.5×10^{-3} nm³ for chiral volumes were imposed.

Cluster analysis. We adopted a statistical clustering technique in order to identify recurring conformations within the large number of structures in an automated manner (Manetti et al., 1995). The purpose of cluster analysis is to place structures into groups or clusters suggested by the data, not defined a priori, such that structures in a given cluster tend to be similar to each other, and structures in different clusters tend to be dissimilar. A set of points, called cluster seeds, was selected as a first guess of the means of the cluster. Each structure was assigned to the nearest seed to form a temporary cluster. The seeds were then replaced by the means of the temporary clusters, and the process was repeated until no further changes occurred in the cluster.

In order not to superimpose with a hierarchical structure the data field, we decided to adopt an agglomerative non-hierarchical method of clustering (*k*-means) (Hartigan, 1975; MacQueen, 1967). This algorithm was applied considering the distance matrix between all pairs of spatial structures as a unit-variable matrix (Sneath, 1983). As a consequence, the distance values actually used by the algorithm are more correctly interpreted as secondary distances; this approach has been demonstrated in many fields of application (Benigni and Giuliani, 1993; Shepard, 1980) to be very useful to single out the patterns embedded in a data field.

The maximum number of clusters was chosen as constraint, since we suppose that this choice is much softer than the radius of clusters (Karpen et al., 1993). Many attempts of dissection were performed, with a different maximum number of clusters, and the actual dissection was performed using the *R*² criterium. In fact *R*² is a good measure of how much of the variation in the data is explained by the model (Bliss, 1967). It is worth noting that the actual value of *R*² is extremely sensitive to the number of clusters. *R*² values are directly comparable with the curves of maximum root-mean-square deviation (RMSD) as a function of the target function cut-off values (Widmer et al., 1993). In this case, the trend of the *R*² values as a function of

Table 1. Amino acid and N-terminal residue chiral analyses of the syringopeptin 25-A. n.d. = not determined.

Fragment	Xaa 1	D-Pro	D-Ser	D-Ala	L-Ala	D-Val	L-Val	D-A ₃ bu	L-A ₃ bu	L-Tyr	D-aThr	D-Leu
A		0.5 (1)	0.9 (1)	6.9 (7)	2.0 (2)	2.3 (3)	1.7 (2)	0.2 (1)	0.7 (1)	0.1 (1)	0.9 (1)	0.9 (1)
B		0.5 (1)	0.9 (1)	6.9 (7)	2.0 (2)	2.3 (3)	1.7 (2)	0.2 (1)	0.7 (1)	0.1 (1)	0.9 (1)	0.9 (1)
C	D-Pro	0.4 (1)		3.0 (3)	0.9 (1)	0.8 (1)	0.8 (1)					0.4 (1)
D	D-Pro	0.9 (1)			1.0 (1)	1.1 (1)						
E	D-Pro	0.9 (1)				1.0 (1)						
F	D-Ala	n.d.										
G	D-Leu			1.0 (1)								0.7 (1)
H	D-Ala		0.7 (1)	4.7 (5)	1.0 (1)	1.6 (2)	1.0 (1)	0.4 (1)	0.5 (1)		1.0 (1)	
I	D-Ala		0.4 (1)	5.0 (5)	0.7 (1)	1.7 (2)	0.9 (1)	0.4 (1)	0.2 (1)	0.1 (1)	0.8 (1)	
J	D-Ala		0.4 (1)	2.0 (2)	0.7 (1)		0.8 (1)	0.3 (1)	0.6 (1)	0.2 (1)	0.7 (1)	
K	L-A ₃ bu	n.d.										

the number of classes, and the observation of the structural differences between the classes, drove the dissection.

Molecular dynamics simulation. Molecular dynamics calculations *in vacuo* were performed with programs from the Groningen molecular simulation (GROMOS) software package (van Gunsteren and Berendsen, 1987). The applied empirical potential energy function contains terms representing bond angle bending, harmonic dihedral angle bending (out-of-plane, out-of-tetrahedral configuration), sinusoidal dihedral torsion, van der Waals and electrostatic interactions (Åqvist et al., 1985). For the sinusoidal dihedral torsion around $-C\alpha-CO-$ of 2,3-dehydro-2-aminobutyric acid, that has a partial double bond character, an energy barrier of $23.0 \text{ kJ} \cdot \text{mol}^{-1}$ was chosen. A dielectric permittivity, $\epsilon = 1$, was used and the cut-off radius of 0.8 nm for the nonbonded interactions was chosen. An attractive half-harmonic restraining potential was applied to force the molecule to satisfy selected NOE distances (Kaptein et al., 1985):

$$V_{\text{OR}}(d_{kl}) = 1/2 k_{\text{dr}}(d_{kl} - d_{kl}^*)^2 \quad \text{if } d_{kl} \geq d_{kl}^*$$

$$V_{\text{OR}}(d_{kl}) = 0 \quad \text{if } d_{kl} < d_{kl}^*$$

where d_{kl} is the actual distance between atoms k and l , d_{kl}^* is the reference distance and k_{dr} is the force constant equal to $4000 \text{ kJ} \cdot \text{mol}^{-1} \cdot \text{nm}^{-2}$.

In order to translate the NOE information into distance ranges, d_{kl}^* , an upper limit of 0.30, 0.35, 0.40, 0.45 and 0.50 nm for strong, medium/strong, medium, medium/weak and weak NOEs, respectively, was chosen (Kaptein et al., 1988). For the evaluation of this potential all protons were treated explicitly. For all other terms only protons attached to nitrogen or oxygen atoms were treated explicitly.

A bond stretching term was not included in the calculation; the SHAKE (Ryckaert et al., 1977) algorithm was used to constrain bond lengths. Several simulated annealing procedures were performed. The initial conformation of each MD simulation was obtained by the DG calculations. Each simulation started with initial velocities obtained from a Maxwellian distribution at the desired temperature. The rescaling of the temperature during the run was obtained by coupling with an external bath (Berendsen et al., 1984). A time step of 2 fs was used in the simulation.

A first 15-ps simulation at $T = 1000 \text{ K}$ was performed with inclusion of the restraining potentials that accounted for the experimental NOEs. To avoid the *cis-trans* peptide isomerization at this temperature (Bruccoleri and Karplus, 1990) a dihedral angle restraining potential was included in the force field; this was sufficient to maintain the *trans* conformation of the peptide bond. Analogous restraining potentials were included for the χ_1 angles of the 2,3-dehydro-2-aminobutyric acid residues. A simulated annealing (Kirkpatrick et al., 1983) procedure was then

performed and the system reached the final temperature $T = 300 \text{ K}$ in 60 ps time. Finally, the system was equilibrated at 300 K for 100 ps. The last 50 ps were used for analysis. The simulation at $T = 300 \text{ K}$ was performed without the torsion angles restraining potentials.

RESULTS

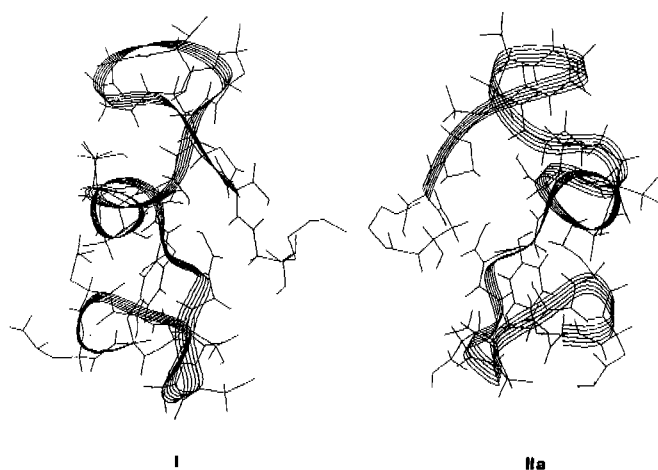
Chirality determination of the amino acid residues of syringopeptins 22-A and 25-A. Partial acid hydrolysis of both lipodepsipeptides yielded a mixture of peptides which was fractionated by RP-HPLC. Purified peptides were sequenced by Edman degradation according to Scaloni et al. (1994) and the stereochemistry of their amino acid residues was determined by chiral analysis according to Marfey (1984) and to Scaloni et al. (1991) for individual amino acids and for N-terminal residues, respectively. The results for 25-A, summarized in Tables 1 and 2, identify the stereochemistry of all residues with the exception of the alternative assignment of D-Ala and L-Ala to position 20 and 22; preference for D-Ala in position 20 and L-Ala in position 22 was motivated by the unambiguous assignment of these residues in the homologous lipodepsipeptide 22-A. The complete stereochemistry of the amino acid residues of this second syringopeptin was deduced from the results summarized in Tables 3 and 4. One step of chiral Edman degradation was necessary to ascertain the configuration of Val3.

NMR spectroscopy. The two-dimensional NMR spectra allowed the individual assignment of all residues and the acquisition of the information necessary for the elucidation of the amino acid sequence and for the determination of the conformation in solution. The experiments were performed both in D_2O and in $\text{H}_2\text{O}/\text{D}_2\text{O}$ (9:1 by vol.). The complete assignment of the resonances was achieved by the TOCSY spectrum which identified all the spin systems of the residues. Particularly, the four resonances present in the olefinic region, showing quartets 1:3:3:1, were straightforwardly assigned to the protons of the four CH groups of 2,3-dehydro-2-aminobutyric acid moiety (Ballio et al., 1991). The assignment of the tyrosine aromatic protons was also straightforward.

In the aliphatic region the assignments resulted from the direct and remote scalar connectivities in TOCSY experiments and from the chemical shift values reported in the literature (Gross and Kalbitzer, 1988). As an example, the characteristic remote connectivities due to the *allo*-threonine (aThr) residue in the TOCSY spectrum were observed with strong coupling of resonances of α and β protons, having cross-peaks with protons of the methyl group. The fingerprint region of the TOCSY spectrum in $\text{H}_2\text{O}/\text{D}_2\text{O}$ (9:1, by vol.) solution indicated the direct

Table 3. Amino acid and N-terminal residue chiral analyses of syringopeptin 22-A. n.d., not determined.

Fragment	Xaa 1	D-Pro	D-Ser	D-Ala	L-Ala	D-Val	L-Val	D-A ₂ bu	L-A ₂ bu	L-Tyr	D-aThr
A		0.6 (1)	0.5 (1)	4.9 (5)	2.0 (2)	2.9 (4)	0.9 (1)	0.1 (1)	0.4 (1)	0.2 (1)	1.0 (1)
B		0.8 (1)	0.6 (1)	5.0 (5)	2.1 (2)	3.5 (4)	1.0 (1)		0.2 (1)		0.9 (1)
C	D-Pro	0.8 (1)		3.0 (1)		2.7 (3)	0.8 (1)				
D	n.d.	0.8 (1)		0.7 (1)		1.0 (1)	0.8 (1)				
E	D-Ala		0.9 (1)	4.3 (4)	2.0 (2)	1.4 (3)			0.6 (1)		0.9 (1)
F	D-Ala		0.2 (1)	3.03 (3)	1.0 (1)	2.6 (3)					0.3 (3)
G	D-Val	n.d.									
H	D-Val		0.7 (1)	2.1 (2)	2.0 (2)	0.9 (1)			0.3 (1)		1.0 (1)
I	D-Ala		0.5 (1)	1.7 (2)	1.0 (1)			1.1 (1)	0.4 (1)	0.1 (1)	1.0 (1)
J	D-Ala		0.7 (1)	2.0 (2)	0.8 (1)			0.2 (1)	0.6 (1)		1.1 (1)
K	D-Ser		0.2 (1)	1.0 (1)	0.8 (1)			0.1 (1)	0.2 (1)	0.1 (1)	
L	D-Ser		0.3 (1)	1.0 (1)	0.6 (1)				0.5 (1)		
M	D-Ala			0.7 (1)	1.0 (1)				0.2 (1)		
N	L-Ala				1.0 (1)			0.9 (1)	0.4 (1)	0.1 (1)	
O	L-A ₂ bu							0.2 (1)	1.0 (1)	0.1 (1)	
P	D-Pro										chiral degradation 1st step: D-Val

**Fig. 3.** Three-dimensional structure of classes I and IIa obtained for syringopeptin 25-A by DG calculations from NMR data as reported in Materials and Methods.

aqueous solution, simulated by a linear combination of four basis spectra (α -helix, β -sheet, random coil and β -turn) according to the method of Chang et al. (1978), showed the presence of a contribution from α -helical forms. For the spectrum in 2,2,2-trifluoroethanol/H₂O (4:1, by vol.), the amount of left-handed α -helix was calculated to be 15% and of β -turn 11%. Previous studies reported a high content of β -turns associated with the presence of dehydroamino acids in the primary structure of polypeptides (Pietrzynski et al., 1992).

Computer simulations. The experimental results presented above allowed an approach to the conformation of syringopeptin 25-A in solution by computer simulations applying both DG and MD procedures.

Distance geometry and cluster analysis. DG computation was performed choosing a fully extended and open chain as starting conformation. The ring closure was imposed using appropriate angle and bond restraints. The 70 structures thus generated had different degrees of agreement with the experimental data. The structures could be grouped into two classes by cluster analysis.

For this partition the root-mean-square distance (RMSD) between observations within each class was 0.043 nm and 0.051 nm, respectively, and the distance between the centroids

3.248 nm. The center of each class was defined as the structure nearest to the centroid (means) of the class, with the lowest overall RMSD with respect to other structures of the same class. The centers of the two classes were analyzed with graphic analysis and appeared to be nearly a pseudomirror image of each other, although the correct chirality was entirely maintained on each of the several chiral centers of the molecule. Particularly, it was observed that within class I (24 structures) only the *trans* rotamer was produced for the lactonic ring closure torsion angle, whilst in class II both *cis* (20 structures) and *trans* (26 structures) rotamers were present (classes IIa and IIb, respectively). The structures of *trans* rotamers in both classes did not completely satisfy the imposed constraints within the limit of the allowed tolerance. Some deviation from tolerance was also observed in a limited region of the molecular moiety in close proximity to the lactone closure, thus indicating that the lactone linkage undergoes a slight distortion from planarity. The structures of classes I and IIa are reported in Fig. 3. The following discussion will show that class IIb, although close to class IIa, has the lowest reliability. For this reason it is not included in the figure.

Molecular dynamics simulations. MD simulations were performed starting from the center of each of the three classes obtained by the DG calculations, taken as the most representative conformer of the class.

After simulated annealing, class I showed a transition of the lactone torsion angle into *cis* rotamer and three violations >0.1 nm. Class II still showed a lactone torsion angle in both *cis* and *trans* rotamers (classes IIa and IIb, respectively) with six violations >0.1 nm for the *cis* rotamer and eight for the *trans* rotamer, as reported in Table 8. This shows that the violations of class IIb are localized around the lactone ring closure and indicate that the *trans* torsion angle has a scarcely compatible value.

In order to select a solution conformation, another parameter, not included as a restraint in the simulation, has been taken into account, namely the 3J coupling constant (about 9 Hz) involving the H-C α -C β -H bonds of the aThr18 residue. This J value corresponds to a *trans* conformation with a torsion angle value of about 180°, typical of *cis* rotamers of the lactone dihedral angle. The average values of this angle in the MD simulations were 177° (RMS fluctuation 7°), 197° (RMS fluctuation 7°) and -93° (RMS fluctuation 7°) for class I, IIa and IIb, respectively.

The average potential energy of each class in the MD simulation was 127 ± 28 , 256 ± 26 and 244 ± 28 kJ · mol⁻¹ for classes I, IIa and IIb, respectively. Thus, class I represents a more likely

Table 5. Assignments of resonances of ^1H and ^{13}C NMR spectrum of syringopeptin 25-A. Spectra were obtained as reported in Materials and Methods. Values are measured from tetramethylsilane.

Fatty acid	Atom	Chemical shift of							
		C2	C3	C4	C5	C6-C7	C8	C9	C10
		ppm							
	^1H	2.57, 2.52	4.10	1.52, 1.55	1.28, 1.40	1.2	1.2	1.25	0.84
	^{13}C	43.8	69.5	37.2	25.8	29.5	32.2	23.2	14.5

Amino acid	Atom	Chemical shift of				
		NH	C α	C β,β'	C γ,γ'	C δ,δ'
		ppm				
Dhb1	^1H	9.60	—	5.94	1.78	
	^{13}C			127.0	13.0	
Pro2	^1H	—	4.20	2.38	1.89, 1.98	3.65
	^{13}C		62.0	31.0	26.0	51.0
Val3	^1H	7.96	4.06	2.09	0.93	
	^{13}C		61.0	31.0	19.0	
Ala4	^1H	8.12	4.25	1.38		
	^{13}C		51.0	17–18		
Ala5	^1H	8.05	4.31	1.38		
	^{13}C		51.0	18.0		
Val6	^1H	7.94	4.06	2.09	0.93	
	^{13}C		61.0	31.0	19.0	
Leu7	^1H	8.40	4.28	1.66	1.59	0.83, 0.92
	^{13}C		53.5	40.5	—	21.5, 23.5
Ala8	^1H	8.25	4.30	1.41		
	^{13}C		51.0	18.0		
Ala9	^1H	8.16	4.30	1.49		
	^{13}C		50.8	17.3		
Dhb10	^1H	9.27	—	6.78	1.79	
	^{13}C			136.5	14.0	
Val11	^1H	7.70	4.12	2.21	1.03	
	^{13}C		60.5	31.0	19.7	
Dhb12	^1H	9.50	—	6.70	1.78	
	^{13}C			135.5	13.0	
Ala13	^1H	7.79	4.31	1.38		
	^{13}C		51.0	17.0		
Val14	^1H	8.15	4.06	2.09	0.94	
	^{13}C		61.0	31.0	19.0	
Ala15	^1H	8.53	3.98	1.40		
	^{13}C		51.0	18.0		
Ala16	^1H	8.27	4.31	1.49		
	^{13}C		50.8	17.3		
Dhb17	^1H	9.35	—	6.83	1.79	
	^{13}C			138.0	14.0	
Thr18	^1H	7.99	4.56	5.16	1.21	
	^{13}C		58.5	71.8	17.7	
Ser19	^1H	7.80	4.51	3.84, 3.96		
	^{13}C		56.0	63.0		
Ala20	^1H	8.32	4.31	1.49		
	^{13}C		50.8	17.3		
Val21	^1H	8.25	4.00	2.09	0.97	
	^{13}C		61.5	31.0	19.0	

Table 6. NMR NOE intensity observed. W, M, S = weak, medium, strong (see text). FA = fatty acid.

Pair type	Atom pair	Intensity
$i-(i+1)$	FA C α -1N	S
	FA C4-1N	M/W
	FA C5-1N	M/W
	1N-2 δ	M
	1 β -2 γ	W
	1 β -2 δ	M
	2C α -3N	M
	4C α -5B	W
	5C α -6N	S
	6C α -7N	S
	7 δ -8N	S
	7 γ -8N	W
	8C γ α -9N	S
	9C α -10N	S
	9N-10N	S
	9 β -10N	M/S
	9 β -10 β	W
	10N-11N	S
	10N-11 γ	M
	10N-11 β	M/W
	10 β -11 γ	M/W
	10 β -11N	M/W
	11C α -12N	S
	11N-12N	S
	11 γ -12N	M
	11 β -12N	M
	11 γ -12 β	M/W
	12N-13N	S
	12N-13 β	M/W
	16C α -17N	S
	16N-17N	S
	16 β -17N	M/S
	16 β -17 β	W
	17N-18N	S
	17N-18 γ	M/S
	17N-18 β	W
	17 γ -18N	S
	18N-19N	M
	18N-19 α	W
	18 β -19N	W
	18 γ -19N	M
	19C α -20N	M
	19N-20N	M
	19 β -20N	S
	19 β -20N	M/W
	20C α -21N	M
	20 β -21N	M
20N-21 γ	M/W	
21C α -22N	S	
21N-22N	S	
21 γ -22N	S	
21 β -22N	M	
22C α -23N	M	
22 β -23N	M	
23C α -24N	M	
24C α -25N	M	
24N-25N	M	
25 m -18 γ	W	
25 m -18N	M/W	
25 o -18 γ	W	
25 o -18N	W	
$i-(i+2)$	9 α -11N	M
	9 β -11N	M/W
	10N-12N	W
	11 γ -13N	W
	16 β -18N	M/S
18N-20N	W	

Table 6. (continued).

Pair type	Atom pair	Intensity
$i-(i+2)$	20N-22N	W
	20 α -22N	W
	22N-24N	W
	22 β -24N	M/W
	23 γ -25 m	W
$i-(i+3)$	3N-6N	M/W
	9 α -12N	M
	9 β -12N	W
	10 β -13N	W
	11 γ -14N	M/W
	13N-16 β	M/W
	25 o -16 β	W
$i-(i+4)$	3N-7N	M
	12 β -16 β	W
	13N-17N	W

Table 7. Long-range NMR NOE intensity observed. W, M, S = weak, medium, strong (see text). FA = fatty acid.

Atom pair	Intensity
FA C α' -17N	W
1N-17N	M/W
2 γ -12 β	W
2 γ -17 β	W
4N-11 β	W
4N-15N	M/W
5N-11 β	W
11N-23 γ	M
13N-23 α	M

conformational rigidity along the peptide chain, and the presence of alternating heterochiralities, which produces a conformational preference for turns (Wilmot and Thornton, 1988). The sequence and chirality of residues are reported in Fig. 1 and in Tables 1 and 2, respectively, and the conformational features of the molecule in Fig. 4. The long left-handed helicoidal folding from residues 8 to 15 is in agreement with the expected propensity of Ala-like residues to promote helicoidal conformations. The D chirality of all residues of this moiety promotes a left-handed winding. Despite the helix-forming propensity of its side chain (Li and Deber, 1992), DLeu7 is excluded from this structured region, probably in consequence of the heterochiral junction with LVal6.

Leaving aside for the moment Dhb1 located in the initial part of the peptide chain, the residues Dhb10, Dhb12 and Dhb17 play a definite role in determining the solution structure of syringopeptin 25-A. In the ribbon representation of Fig. 4 the occurrence in their position of very narrow turns is quite clear. The effect is particularly great in position 10, whilst is less evident in positions 12 and 17 where the region is largely distorted from a pure helix.

The turns 20-21 and 23-24 located in the lactone moiety are the consequence of heterochiral junctions. The supplementary constraints and the violation of the peptide geometry introduced by the ring closure prevent a precise classification of the turns in terms of classical secondary structure, a situation common to several ring-containing peptides (Rizo and Gierash, 1992, and references cited therein). However, for the sake of simplicity,

Table 8. Violations: NOE effects observed in the NOESY spectra. The relative intensity is reported as strong, medium and weak as defined in Materials and Methods. The internuclear distances obtained by molecular dynamics simulation are also reported. (V), virtual atom(s). The distance restraint interaction refers to a non-atomic calculated site, center of interaction. Strong, medium, weak distances referred to virtual atoms imply a correction term (up to 0.1 nm) which must be added to the allowed proton-proton distances.

NMR NOE	NMR NOE intensity	Molecular dynamics average distance (rms fluctuation) for					
		class I		class IIa		class IIb	
nm							
Dhb1 β -Pro2 γ	W	-	-	(V) 0.60	(0.02)	(V) 0.60	(0.02)
Dhb1 NH-Dhb17 NH	M/W	-	-	0.50	(0.03)	0.50	(0.03)
Val3 NH-Leu7 NH	M	0.51	(0.03)	-	-	-	-
Ala9 α -Dhb12 NH	M	-	-	0.52	(0.03)	0.52	(0.03)
Val11 NH-A ₂ bu23 γ	M	(V) 0.55	(0.03)	(V) 0.58	(0.03)	(V) 0.57	(0.04)
Ala13 NH-A ₂ bu23 α	M	-	-	0.51	(0.03)	0.51	(0.04)
Ala13 NH-Dhb17 NH	W	-	-	0.66	(0.03)	0.68	(0.02)
Dhb17 NH-Thr18 γ	M/S	-	-	(V) 0.50	(0.02)	(V) 0.62	(0.02)
Dhb17 γ -Thr18 NH	S	(V) 0.52	(0.01)	(V) 0.79	(0.03)	(V) 0.51	(0.01)
Thr18 γ -Tyr25 <i>m</i>	W	-	-	-	-	(V) 0.82	(0.03)
Tyr25 <i>m</i> -A ₂ bu23 γ	W	-	-	-	-	(V) 0.81	(0.05)

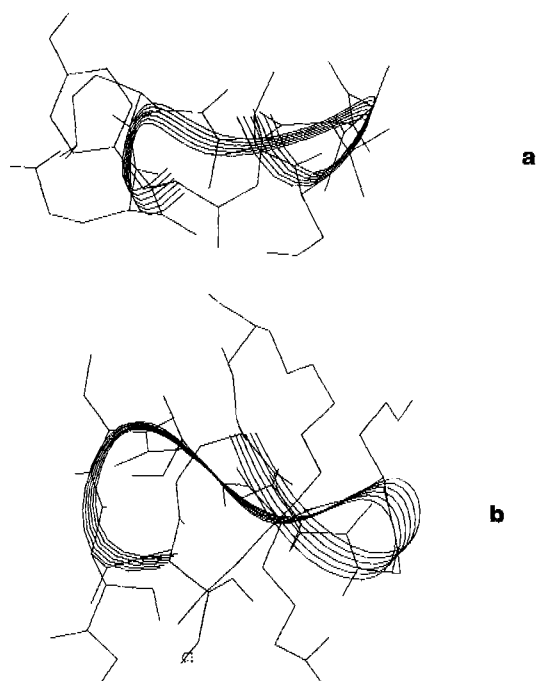


Fig. 6. Comparison between the three-dimensional structures of the lactone rings of syringopeptin 25-A (a) and of syringotoxin (b) respectively.

the turns present in syringopeptin 25-A have been labelled with the same prefixes used for those currently occurring in proteins and homochiral peptides, having the highest similarity. As shown in Fig. 6, the two turns present in the ring are very similar to those found in syringotoxin, another *P. syringae* pv. *syringae* lipodepsipeptide (Gonzales et al., 1981; Fukuchi et al., 1990, 1992; Ballio et al., 1990) recently investigated by MD methods (Ballio et al., 1994). This type of ring conformation, resembling the seam of a tennis ball, was found for the first time in a bioactive lipodepsinapeptide produced by *P. reactans* (Mortishire-Smith et al., 1991b).

CD measurements have provided evidence for changes of the secondary structure on passing from a water solution to a

2,2,2-trifluoroethanol/water mixture which mimicks a membrane-like environment.

An interaction of syringopeptin 25-A with biological membranes is suggested by the striking similarity of its activities (Iacobellis et al., 1992; Di Giorgio et al., 1994; and unpublished data) with those of other natural peptides which affect the integrity of natural and artificial membranes (Saberwal and Nagaray, 1994). It is likely that the predominant lipophilic character of the metabolite, resulting not only from the very high percentage of hydrophobic amino acid residues but also from the fatty acid chain, is the prerequisite for this interaction. The Dhb1 and Pro2 residues can be considered as a hinge across the two lipophilic domains, capable of modulating the local rigidity and thus improving the interaction. This might also be influenced by the likely association of the cationic C-terminal cyclic region of syringopeptin 25-A with the negative headgroups of the phospholipids.

A recent paper (Clark et al., 1994) has provided evidence of a striking similarity between the structure of polymyxins, a class of membrane-active bacterial antibiotics (Storm et al., 1977), and ranalexin, an antimicrobial peptide isolated from the skin of the American bullfrog, *Rana catesbeiana* (Clark et al., 1994), and structurally related to type 1 brevinins (Simmaco et al., 1994). These compounds share a long hydrophobic tail and a cationic heptapeptide ring at their C-terminus, formed in polymyxins through an amide bond between the C-terminus and the δ -amino group of a 2,4-diaminobutyric acid residue, and in ranalexin and type-I brevinins through an intramolecular disulfide bond. These features, considered responsible for the disruption of bacterial membrane permeability and thus for antibiotic activity, are also present in syringopeptins; in particular, their octapeptide cationic loop is formed by a lactone ring, which conserves two positively charged residues in identical positions to those in polymyxins, ranalexins and type-I brevinins. It has been claimed that 'the cationic loop and hydrophobic tail shared by ranalexin and polymyxin could represent a fundamental membrane-permeabilizing peptide motif more widely utilized in nature than previously appreciated' (Clark et al., 1994). The finding that the same motif occurs in some bacterial lipodepsipeptides further extends its significance in nature.

Further studies are in progress to measure and calculate the overall dipole moment of syringopeptin 25-A in order to compare this data with those reported for alamethicin-like peptide

trichotoxin A-40, lantibiotics type-A gallidermin and pep5 which are potential-dependent channel-forming peptides (Freund and Jung, 1991; Schwarz et al., 1983; Rizzo et al., 1985). In fact these compounds have a very helicoidal conformation similar to that obtained for syringopeptin 25-A.

Thanks are due to Drs Alessandro Giuliani and Alberto Boffi for helpful discussion about statistical methods and CD analysis. This work has been supported in part by grants of the Italian National Research Council (CNR), special *ad hoc* program *Chimica fine II, Ministero dell'Università e della Ricerca Scientifica e Tecnologica*, and NATO (no. 921129 to A. B.).

REFERENCES

- Åqvist, J., van Gunsteren, W. F., Leijonmarck, M. & Tapia, O. (1985) A molecular dynamics study of the C-terminal fragment of the L7/L12 ribosomal protein, *J. Mol. Biol.* **183**, 461–477.
- Aydin, M., Lucht, N., Koenig, W. A., Iupp, R., Jung, G. & Winkelmann, G. (1985), *Liebigs Ann. Chem.*, 2285–2300.
- Ballio, A., Bossa, F., Collina, A., Gallo, M., Iacobellis, N. S., Paci, M., Pucci, P., Scaloni, A., Segre, A. & Simmaco, M. (1990) Structure of syringotoxin, a bioactive metabolite of *Pseudomonas syringae* pv. *syringae*, *FEBS Lett.* **269**, 377–380.
- Ballio, A., Barra, D., Bossa, F., Collina, A., Grgurina, I., Marino, G., Moneti, G., Paci, M., Pucci, P., Segre, A. L. & Simmaco, M. (1991) Syringopeptins, new phytotoxic lipodepsipeptides of *Pseudomonas syringae* pv. *syringae*, *FEBS Lett.* **291**, 109–112.
- Ballio, A., Collina, A., Di Nola, A., Manetti, C., Paci, M. & Segre, A. (1994) Determination of structure and conformation in solution of syringotoxin, a lipodepsipeptide from *Pseudomonas syringae* pv. *syringae* by 2D NMR and molecular dynamics, *Struct. Chem.* **5**, 43–50.
- Benigni, R. & Giuliani, A. (1993) Analysis of distance matrices for studying data structures and separating classes, *Quant. Struct. Act. Relat.* **12**, 397–401.
- Berendsen, H. J. C., Postma, J. P. M., van Gunsteren, W. F., Di Nola, A. & Haak, J. R. (1984) Molecular dynamics with coupling to an external bath, *J. Chem. Phys.* **81**, 3684–3690.
- Bliss, C. I. (1967) *Statistic in biology*, vol. 1, McGraw-Hill, New York.
- Braunschweiler, L. & Ernst, R. R. (1983) Coherence transfer by isotropic mixing: Application to proton correlation spectroscopy, *J. Magn. Reson.* **53**, 521–528.
- Bruccoleri, R. F. & Karplus, M. (1990) Conformational sampling using high-temperature molecular dynamics, *Biopolymers* **29**, 1847–1862.
- Chang, C. T., Chuen-Shang Wu, C. & Yang, J. T. (1978) Circular dichroic analysis of protein conformation: Inclusion of the α -turns, *Anal. Biochem.* **91**, 13–31.
- Clark, D. P., Durrell, S., Maloy, W. L. & Zasloff, M. (1994) Ranalexin, a novel antimicrobial peptide from bullfrog (*Rana catesbeiana*) skin, structurally related to the bacterial antibiotic, polymyxin, *J. Biol. Chem.* **269**, 10849–10855.
- Crippen, G. M. (1983) in *Chemometric research studies series* (Bawden, D., ed.) Wiley, New York.
- Di Giorgio, D., Camoni, L. & Ballio, A. (1994) Toxins of *Pseudomonas syringae* pv. *syringae* affect H⁺-transport across the plasma membrane of maize, *Physiol. Plant.* **91**, 741–746.
- Freund, S. & Jung, G. (1991), Lantibiotics: An overview and conformational studies on gallidermin and pep5, *NATO ASI Ser. H, Cell Biol.* **65**, 75–92.
- Fukuchi, N., Isogai, A., Nakayama, J. & Suzuki, A. (1990) Structure of syringotoxin B, a phytotoxin produced by citrus isolates of *Pseudomonas syringae* pv. *syringae*, *Agric. Biol. Chem.* **54**, 3377–3379.
- Fukuchi, N., Isogai, A., Nakayama, J., Takayama, S., Yamashita, S., Suyama, K., Takemoto, J. Y. & Suzuki, A. (1992) Structure and stereochemistry of three phytotoxins, syringomycin, syringotoxin and syringostatins, produced by *Pseudomonas syringae* pv. *syringae*, *J. Chem. Soc. Perkin Trans. I*, 1149–1157.
- Gonzales, C. F., DeVay, J. E. & Wakeman, R. J. (1981) Syringotoxin: a phytotoxin unique to citrus isolates of *Pseudomonas syringae*, *Physiol. Plant Pathol.* **18**, 41–50.
- Gross, K.-H. & Kalbitzer, H. R. (1988) Distribution of chemical shifts in ¹H nuclear magnetic resonance spectra of proteins, *J. Magn. Reson.* **76**, 87–89.
- Hartigan, J. A. (1975) *Clustering algorithms*, John Wiley, New York.
- Iacobellis, N. S., Lavermicocca, P., Grgurina, I., Simmaco, M. & Ballio, A. (1992) Phytotoxic properties of *Pseudomonas syringae* pv. *syringae* toxins, *Physiol. Mol. Plant. Pathol.* **40**, 107–116.
- Jeener, J., Meier, B. H., Bachmann, P. & Ernst, R. R. (1979) Investigation of exchange processes by two-dimensional NMR spectroscopy, *J. Chem. Phys.* **71**, 4546–4553.
- Kaptein, R., Zuiderweg, E. R. P., Scheek, R. M., Boelens, R. & van Gunsteren, W. F. (1985) A protein structure from nuclear magnetic resonance data. lac repressor headpiece, *J. Mol. Biol.* **182**, 179–182.
- Kaptein, R., Boelens, R., Scheek, R. M. & van Gunsteren, W. F. (1988) Protein structures from NMR, *Biochemistry* **27**, 5389–5395.
- Karpen, M. F., Tobias, D. J. & Brooks, C. I. III (1993) Statistical clustering techniques for the analysis of long molecular dynamics trajectories: Analysis of 2.2-ns trajectories of YPGDV, *Biochemistry* **32**, 412–420.
- Kirkpatrick, S., Gelatt, C. D. Jr & Vecchi, M. P. (1983) Optimization by simulated annealing, *Science* **220**, 671–680.
- Levitt, M. H., Freeman, R. & Frenkiel, T. A. (1982) Broadband heteronuclear decoupling, *J. Magn. Reson.* **47**, 328–338.
- Li, S.-C. & Deber, C. M. (1992) Glycine and β -branched residues support and modulate peptide helicity in membrane environments, *FEBS Lett.* **311**, 217–220.
- MacQueen, J. B. (1967) Some methods for classification and analysis of multivariate observations, *Proceedings of the Fifth Berkeley Symposium on Mathematical Statistics and Probability I*, 281–297.
- Manetti, C., Fogliano, V., Riteni, A., Santini, A., Randazzo, G., Logrieco, A., Mannina, I. & Segre, A. L. (1995) Determination of the structure of fusaproliferin by ¹H-NMR and distance geometry, *Struct. Chem.* **6**, 183–189.
- Marfey, P. (1984) Determination of d-amino acids. II. Use of a bifunctional reagent, 1,5-difluoro-2,4-dinitrobenzene, *Carlsberg Res. Commun.* **49**, 591–596.
- Marion, D. & Wüthrich, K. (1983) Application of phase sensitive two-dimensional correlated spectroscopy (COSY) for measurements of ¹H-¹H spin-spin coupling constants in proteins, *Biochem. Biophys. Res. Commun.* **113**, 967–974.
- Mortishire-Smith, R. J., Drake, A. F., Nutkins, J. C. & Williams, D. H. (1991a) Left handed α -helix formation by a bacterial peptide, *FEBS Lett.* **278**, 244–246.
- Mortishire-Smith, R. J., Nutkins, J. C., Packman, L. C., Brodey, C. L., Rainey, P. B., Johnstone, K. & Williams, D. H. (1991b) Determination of the structure of an extracellular peptide produced by the mushroom saprotroph *Pseudomonas reactans*, *Tetrahedron* **47**, 3645–3654.
- Nutkins, J. C., Mortishire-Smith, R. J., Packman, L. C., Brodey, C. L., Rainey, P. B., Johnstone, K. & Williams, D. H. (1991) Structure determination of tolaasin, an extracellular lipodepsipeptide produced by the mushroom pathogen *Pseudomonas tolaasii* Paine, *J. Am. Chem. Soc.* **113**, 2621–2627.
- Pietrzynski, G., Rzeszutarska, B. & Kubica, Z. (1992) Conformational investigation of α,β -dehydropeptides. Part IV. β -turn in saturated and α,β -unsaturated peptides Ac-Pro-Xaa-NHCH₃: NMR and IR studies, *Int. J. Peptide Protein Res.* **40**, 524–531.
- Rainey, P. B., Brodey, C. L. & Johnstone, K. (1991) Biological properties and spectrum of activity of tolaasin, a lipodepsipeptide toxin produced by the mushroom pathogen *Pseudomonas tolaasii*, *Physiol. Mol. Plant Pathol.* **39**, 57–70.
- Rizo, J. & Gierasch, L. M. (1992) Constrained peptides: models of bioactive peptides and protein substructures, *Annu. Rev. Biochem.* **61**, 387–418.
- Rizzo, V., Schwarz, G., Voges, K.-P. & Jung, G. (1985) Molecular shape and dipole moments of alamethicin-like synthetic peptides, *Eur. Biophys. J.* **12**, 67–73.
- Rose, G. D., Gierasch, L. M. & Smith, J. A. (1985) Turns in peptides and proteins, *Adv. Protein Chem.* **37**, 1–109.
- Ryckaert, J. P., Cicotti, G. & Berendsen, H. J. C. (1977) Algorithms for macromolecular dynamics and constraint dynamics, *Mol. Phys.* **34**, 1311–1327.
- Saberwal, G. & Nagaraj, R. (1994) Cell-lytic and antibacterial peptides that act by perturbing the barrier function of membranes: facets of

- their conformational features, structure-function correlations and membrane-perturbing abilities, *Biochim. Biophys. Acta* 1197, 109–131.
- Scaloni, A., Simmaco, M. & Bossa, F. (1991) Determination of the chirality of amino acid residues in the course of subtractive Edman degradation of peptides, *Anal. Biochem.* 197, 305–310.
- Scaloni, A., Barra, D. & Bossa, F. (1994) Sequence analysis of dehydroamino acid-containing peptides, *Anal. Biochem.* 218, 226–228.
- Schwarz, G., Savko, P. & Jung, G. (1983) Solvent dependent structural features of membrane-active peptide trichotoxin A-40 as reflected in its dielectric dispersion, *Biochim. Biophys. Acta* 728, 419–428.
- Shepard, R. N. (1980) Multidimensional scaling, tree-fitting, and clustering, *Science* 210, 390–398.
- Simmaco, M., Mignogna, G., Barra, D. & Bossa, F. (1994) Antimicrobial peptides from skin secretions of *Rana esculenta*, *J. Biol. Chem.* 269, 11956–11961.
- Sneath, P. H. A. (1983) Distortions of taxonomic structure from incomplete data on a restricted set of reference strains, *J. Genet. Microbiol.* 129, 1045–1073.
- Storm, D. R., Rosenthal, K. S. & Swanson, P. E. (1977) Polymyxin and related peptide antibiotics, *Annu. Rev. Biochem.* 46, 723–763.
- van Gunsteren, W. F. & Berendsen, H. J. C. (1987) *Groningen molecular simulation (GROMOS) library manual*, Biomos, Groningen.
- Widmer, H., Widmer, A. & Braun, W. (1993) Extensive distance geometry calculations with different NOE calibrations: New criteria for structure selection applied to Sandostatin and BTPI, *J. Biomol. NMR* 3, 307–324.
- Williamson, M. P., Havel, T. F. & Wüthrich K. (1985) Solution conformation of proteinase inhibitor IIA from bull seminal plasma by ¹H nuclear magnetic resonance and distance geometry, *J. Mol. Biol.* 182, 295–315.
- Wilmot, C. M. & Thornton, J. M. (1988) Analysis and prediction of different types of β -turn in proteins, *J. Mol. Biol.* 203, 221–232.
- Wüthrich, K., Billeter, M. & Braun, W. (1983) Pseudo-structures for the 20 common amino acids for use in studies of protein conformations by measurement of intramolecular proton-proton distance constraints with nuclear magnetic resonance, *J. Mol. Biol.* 169, 949–961.